GDR in Radiotherapy Treatment Fields with 18 MV Accelerators

R. R. Martín-Landrove[1], J. Dávila[1], H. R. Vega-Carrillo[2], M. T. Barrera[3], A.J. Kreiner[4], F. Pino[3], H. Barros[3], E. D. Greaves[3] and L. Sajo-Bohus[3]*
[1]Universidad Central de Venezuela and Física Médica C. A., Caracas, Venezuela
[2]Universidad Autónoma de Zacatecas, Unidad Académica de Estudios Nucleares, C. Ciprés 10, Fracc. La Peñuela, 98068 Zacatecas, Zac. México
[3]Universidad Simón Bolívar, Nuclear Physics Laboratory, Sartenejas, Caracas, Venezuela
[4]Departamento de Física, CNEA, Buenos Aires, Argentina. Escuela de Ciencia y Tecnología, Universidad Nacional de San Martín, San Martín, Argentina y CONICET, Argentina.
* Visiting Professor at the University of Padova, Italia

Abstract
Giant dipole photo-nuclear reactions generated during Linac radiotherapy are of concern due to the undesirable neutron dose delivered to patients. Nuclear track methodology provides an estimation of gradients of photo-neutrons fields in radiotherapy treatments for 18 MV linear accelerators and it revealed an unexpected behaviour around isocenter. Enhancement effects are observed on absorbed dose due to both scattered photo-neutrons and (γ,n) reactions. Thermal neutrons can give a dose boost if the tumour is loaded with ^{10}B and a new BNCT approach combined with the standard photon field is proposed.

1 Introduction

Energetic gamma rays or bremsstrahlung photons interacting with highly deformed nuclei produce photo-neutrons mainly related to high-frequency collective excitation. Photo-neutrons energy window is defined by reaction mechanisms and for a given energy window, nucleons and mostly neutrons, break free during photo-nuclear and electro-nuclear reactions. Photons impinging on heavy targets such as tungsten, lead and iron produce photo-neutrons with a well established spectrum and in that sense, Liu et at. [1] reported giant-dipole-resonance photo-neutrons (GRN) produced by a clinical medical accelerators (Varian Clinac 2100C/2300C). Photo-neutron contributions produce an additional gamma-radiation dose delivered to the patients during radiation treatment. It is expected that the neutron dose is not negligible and it should be in principle determined for every single radiotherapy facility working with clinical linear accelerators working at operating potentials above 10 MV. A proper estimation of the in-field contribution to the absorbed gamma dose, which is the dominant one, requires an adequate knowledge of the neutron spectrum. Simulations by Monte Carlo methods provide information on expected photo-neutron production, neutron spectrum and diffusion in materials under realistic geometries related to patient, accelerator material and accessories. For practical reasons the choice for passive detectors with two energy windows in the thermal and epithermal energy range for the neutron spectrum was made. Further refinements were acomplished by Monte Carlo simulation in order to confirm the measurements made by nuclear track methodology (NTM) using polyallyl diglycol carbonate (PADC), which are passive detectors type CR-39^{TM}.

2 Photo-neutron production during radiotherapy with high energy linear accelerators

The photo-nuclear interaction between bremsstrahlung radiation and heavy nuclei leads to the breaking of neutron-nucleus bound system and releasing a photo-neutron. Within the tungsten target photons produce photo-neutron reactions in the accelerator target, shielding, collimators and equipment materials. Some metals with threshold energies in the MeV region like Al (13.06), Fe (7.65), Au (8.06), Pb (8.09), W (6.19) are involved [2]. Also, neutrons are produced by virtual photon reactions that take place in the tungsten target and their frequency depends mainly on the structural materials of linear accelerator heads. Kase et al. [3] reports that 35% of production takes place at the primary collimator. Furthermore, photo-neutrons could reach the surrounding matter inducing neutron activation. Consequently some radioisotopes will decay, through prompt and delayed gamma-rays. Thus, in principle, the patient and staff may receive an undesirable dose [4] increasing the lifetime probability risk for oncogenesis; photo-neutron energies between 5.6 and 18 MeV may induce significant dose equivalents to critical organs [5].

3 Simulation of neutron production and transport

Several studies have been reported with the aim of determining the neutron spectra in the treatment halls with linear accelerators. Neutron spectra are measured with a Bonner sphere spectrometer with a passive neutron detector, or the dose is obtained through the linear energy transfer spectrum of recoils in CR-39^{TM} plastic nuclear track detectors. Some work also includes the Monte Carlo calculation of neutron spectra and the dose [8]. A review on photoneutron characteristics in radiation therapy with high-energy photon beams are given elsewhere [9-11,1]. Our study is oriented to determine the photo-neutron gradient around the isocenter for a medical linear accelerator operating at 18 MV. A model of the accelerator head and vault was used with the MCNP5 code [12]. The program runs a large number of histories for every particle and so significant computing time is necessary to obtain good statistics. Several methods exist to overcome this drawback and one of them is offered by the code called the F5 tally [13]. Following the F5 tally, neutron spectra and room dose equivalent were calculated in several points inside the accelerator vault. Also, calculations at different locations on the treatment couch were carried out. The amount of histories was large enough to have uncertainties less than 3% on the location point for every detector. To handle the photo-neutron source term during the simulation we follow Tossi et al. [14] approach which takes into account the contribution due to evaporation and neutrons produced by the knock on reaction mechanism. The source term was allocated on the target and the accelerator head was modelled as a spherical shell made of W, Fe and Pb. The isocenter was located on the treatment couch which was modelled as made out of carbon fiber.

4 Nuclear track-etching methodology for photo-neutron detector

The CR-39^{TM} is particularly useful for charged particle detection in the linear energy transfer (LET) range above the threshold value of ~10 keV. Photo-neutrons can be detected through latent tracks induced in PADC by proton and heavier nuclei recoils or charged reaction products. The method is characterized by short irradiation times of around 40 s at 600MU/min. To deploy detectors with a proper positioning and to prepare the irradiation configuration takes a few minutes. This is an important advantage over other techniques based on active systems, which require a whole day of activity. Exposed detectors to photo-neutrons and scattered neutrons at the photon-beam isocenter, provide useful

information on the existing neutron field for patients undergoing, for instance, prostate treatment. In this case, using the Intensity-Modulated Radiation Therapy (IMRT) as an advanced radiotherapy modality has the main advantage of smaller expected side effects as compared with conventional radiotherapy. On the other hand, it has also been shown that collimators made out of W, Fe and Al, increase photo-neutron production rate so that an additional dose is expected. The NTM to be considered combines CR-39^{TM} with converters and neutron fields are determined indirectly by charged fragments from a $^{10}B(n,\alpha)$ reaction. The high LET products (He^{++} and $^{7}Li^{+}$) leave their kinetic energy in the PADC where a large number of atoms ionize, and before electronic recombination takes place; the resulting electronic avalanche extends ionization to about 1000 nm far away from the impinging direction. To produce latent tracks related to thermal and fast neutrons, the detector surface is covered with highly enriched ^{10}B boric acid with or without a 0.8 mm thick cadmium cover. The resultant size and shape of the damaged volume depends on the absorbed ion energy, mass and momentum and it is visible in CR-39^{TM} after chemical etching (6N, NaOH, 70^{o}C) under light transmission microscope (10 x 40). Tracks of the order of micrometers are visible and their diameters are measure and collected in histogram bars.

5 Expected photo-neutron dose during radiotherapy

An important feature for a radiation detector is that it should produce a minimal distortion of the observed radiation fields. In that sense CR-39^{TM} is quite adequate when used for dosimetry purposes in radiotherapy. Minimal distortion can be assured if its radiation transport properties are not very different from those of surrounding tissues and in that sense CR-39^{TM} can be considered equivalent to skin and/or adipose tissue. Measurements show that, for photons, the difference of total mass attenuation coefficients for adipose tissue and CR-39^{TM} was under 3.5 % in the 5-20 MeV range and it falls quickly in the high energy range. In the case of electrons the difference of mass stopping powers for skin and CR-39^{TM} was under 4 % and it is nearly constant in the same energy range. In principle these results indicate that the detector can be placed on the patient's skin for external in vivo dosimetry. When neutron transport is considered, the hydrogen atom density is the relevant quantity to be compared for CR-39^{TM}, adipose tissue and skin. It turns out that these densities have very similar values. In Fig. 1 we report the difference Photon mass attenuation coefficients and Electron mass stopping power in the 5-20 MeV range for CR-39^{TM} - adipose tissue and CR-39^{TM} - skin respectively. For the absorbed dose evaluation a good knowledge of neutron fluence as a function of the energy is required as input information. In principle such evaluation is beyond the scope of this work because our experimental array provides a measurement of integrated neutron fluxes for three energy windows. Nevertheless, the neutron fluxes calculated from simulation of neutron production and transport in the presence of a water tank phantom [15] compared with those related to nuclear-track detectors

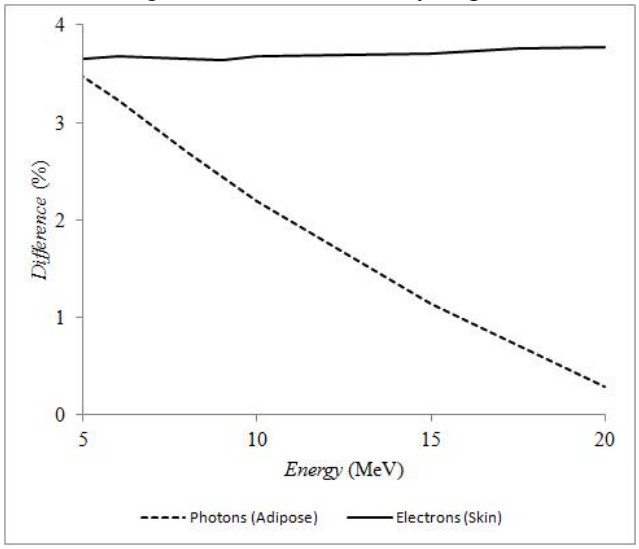

Fig. 1. Difference in the 5-20 MeV range of: (a) Photon mass attenuation coefficients (dotted line) for CR-39^{TM} and adipose tissue. (b) Electron mass stopping power (solid line) for CR-39^{TM} and skin.

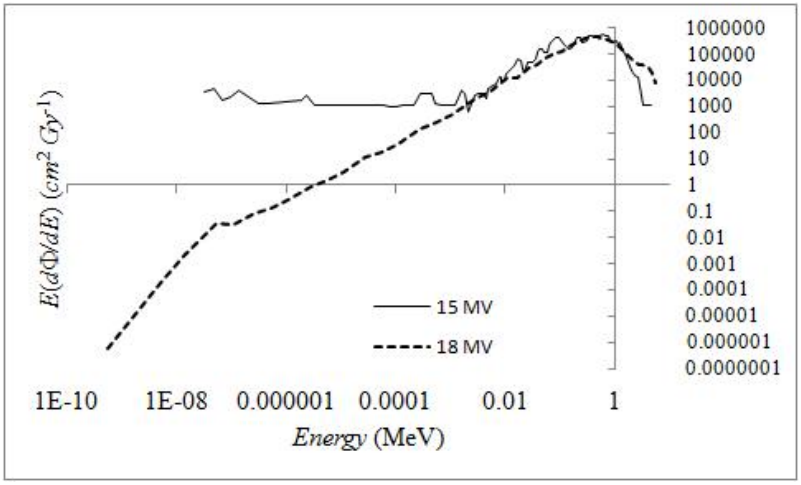

Fig.2. Comparison of simulations where neutron fluence is a function of letargy for two experiments with photon beams (10x10cm^2 field): (a) CR-39^{TM} detector irradiation at isocenter (dotted line). (b) Water tank phantom irradiation at isocenter (solid line). This comparison is still relevant in spite of accelerator operational voltage difference because the delivered dose should be the same in compliance to medical standards. The remarkable features are an important suppression of fluence in the thermal neutron energy range for CR-39^{TM} and a nearly perfect overlap in the fast neutron energy range.

alone allow the evaluation of the role of thermal neutrons coming from the patient for the absorbed dose build-up. In Fig. 2 a comparison is made for such simulations and it can be seen that for the same dose delivery at isocenter (which is achieved in both cases to comply with medical standards, regardless the particular features of each accelerator) there is a remarkable difference in the thermal neutron energy range and a nearly perfect overlap in the fast neutron energy range. The bigger contribution of thermal neutrons is due to the presence of the patient or the water tank phantom in this case. The probability distributions of non-elastic interactions are depicted in Fig. 3 and in all of them the main contribution is related to the thermal neutron energy range. The absorbed dose break-down per delivered Gy at isocenter is shown in Table I for breast tissue. The dominant contributions correspond to (n,γ) and (n,p) reactions and if we take 0.5 MeV as the top energy for thermal neutrons, they deliver 86.1% and 56.6% of the absorbed dose for each channel, which implies that for the in-field case most of the absorbed dose is induced by the patient. Clearly the presence of a patient is paramount for thermal neutron production and it should be related to the fact that the patient's body has very high hydrogen content. The lifetime probability risk for oncogenesis is shown in Table II [16-17]. In terms of a risk/benefit basis it does not pose a significant risk although it is advisable to avoid this kind of treatments in children.

6 Experimental Details and Results

The experimental set-up used in our measurements consists of a passive detector with different assembled configurations i.e. bare, lined with and without Cd-filter. The Linac was operated at a nominal voltage of 18 MV for a time of 39.6 s, for a total dose of 400 MU and a dose rate of 600 MU/min (MU, monitor unit, corresponds to 1cGy in a field of 10x10 cm² in the Dmax point at 3.2cm depth in water). Detectors were placed at different locations on the treatment couch and the origin of the reference system corresponds to the isocenter. Fig. 4 shows comparison between simulated and measured data.

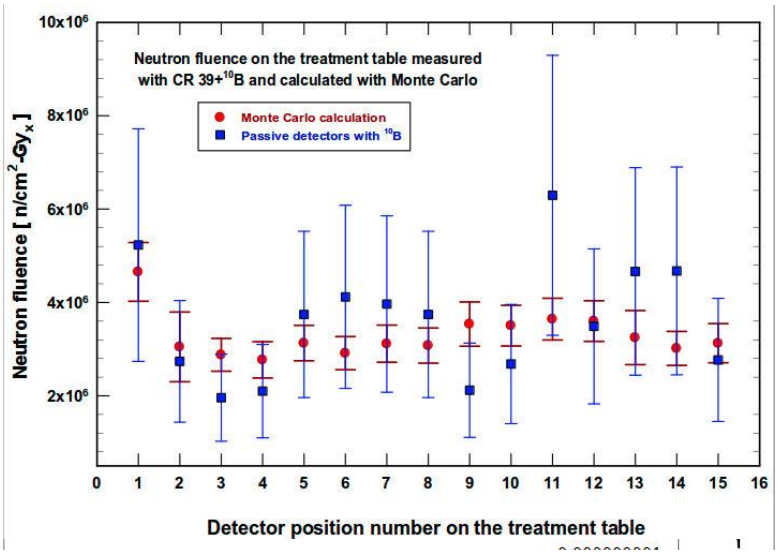

Fig. 4. Neutron fluence on the treatment couch measured with ^{10}B+CR-39 and simulalated with Monte Carlo. Passive detectors results are shown by squares.

Fig. The contribution from the thermal neutron energy range is going to play a leading role in dose build-up.

Table I: Absorbed dose break-down (mGy) per delivered Gy at isocenter

Total	γ from (n,γ)	β^a	γ after β^a	(n,α)	(n,p) Inelastic	(n,p) Elastic
0.357	0.225	0.012	0.004	0.022	0.003	0.091

[a] Accumulated dose 50 years after irradiation.

Table II: Lifetime probability risk for oncogenesis (%, 30 Gy treatment) by age[a]

Source	5 years	20 years	40 years	60 years	80 years
ICRP 60	0.150	0.086	0.032	0.021	0.005
BEIR V	0.150	0.123	0.064	0.054	0.021

[a] For breast tissue (ICRU-44)

7 Discussion

As a first result it was found that detectors without neutron converter show tracks of small area due to recoils; these are mainly protons produced by (n, p) reactions due to thermal or fast neutrons. The track distribution is shown at the top in Fig.6, around channel 5 it shows a maximum and then it decreases as a nearly exponential curve to negligible values as get closer to the channel where heavy ions are expected to be recorded. Few large tracks above channel 25 are shown but these are due to heavy nuclei recoils (PADC oxygen and carbon). We do not expect to observe tracks related to cosmic ray particles due to the short exposure time of the PADC-NTD. The proton track spectrum is subtracted from the histograms of those that are related to PADC-covered with a ^{10}B-converter and a Cd-filter. The resulting histogram is free from tracks related to proton recoils and it shows a peak produced by alpha-tracks as a product of the photo-neutron reaction ^{10}B(n,α). The amount of alpha tracks from PADC lined by Cd is less than those without a Cd-filter. This result is explained by the ^{10}B(n,α) reaction cross section (~3838 b) for

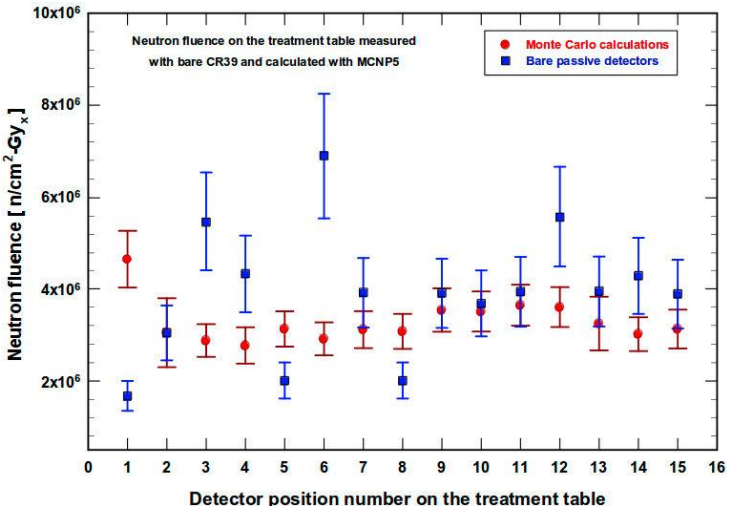

Fig.5. Neutron fluence on the treatment table measured with bare CR-39^{TM} (only proton tracks) and determined by Montecarlo simulation.

thermal neutrons but still has high value in the neutron resonance energy region (assured by the Cd-filtering property).

Therefore, the spectral difference is related to alpha-tracks from photo-neutrons with energy above the thermal region. Similar procedure to determine spectral differences are applied to the whole set of detectors positioned around the treatment couch. The results provide data to draw a photo-neutron field map indicating the intensity gradient of thermal and fast neutron region.

This result is important when a dosimetric evaluation should be performed for a shielding geometry assessment. Three other results were obtained, the first is the simulation to determine the neutron fluence around the treatment couch. The next is the agreement between the PADC detector track density with the one predicted by Monte Carlo, as it is shown in Fig. 4. The latter is related to an effect not reported so far which can be determined comparing expected neutron fluence with track density at the same spot. The outcome (see Fig. 7) is that as we depart from the isocenter on the treatment couch the neutron fluence decreases sharply first and then it slowly increases to maintain a steady value. This has not been reported so far in the literature and it could be an important result that needs to be studied in detail in order to have a better control of neutron dose.

8 Conclusions

The experiments were carried out at a radiotherapy facility with a Varian Clinac 2300 accelerator and the goal was to determine the photo-neutron fluence and its gradient. The track distributions are due to proton recoils and alphas particles produced by photo-neutrons. The NTM was used advantageously by the combination of CR-39^{TM} with neutron converters and cadmium filters to determine the photo-neutron field in a radiotherapy hall and it leads to similar results already obtained by other authors with different approaches. Monte Carlo simulations give some hint on the expected neutron dose gradient during treatments. As a byproduct, enhanced effect on the absorbed dose due to both scattered neutrons and by (γ,n) reactions, could be considered as a relevant processes to improve tumor treatment. The possibility exists for thermal neutrons to give a dose boost if the tumor is previously loaded with ^{10}B.

We observed the existence at the isocenter of a non uniform photo-neutron dose rate. The calculated photo-neutron fluence has a value comparable with current BNCT practice. Hence the two effects overlap and could be used for therapy with the combination of standard phototherapy and boron photo-neutron capture therapy (BPNCT) as a new approach in glioblastoma multiforme treatment. This is a new possibility not yet discussed in the literature. A deconvolution technique, for thermal and fast neutron discrimination and gradient determination has not been reported in literature as well and it could be considered a new procedure in neutron spectrometry by NTM.

Acknowledgement

The authors are grateful to Erik Salcedo (M.Sc.) for his skillful help during Linac operation and detector exposure, as well as to the GURVE Radiotherapy Center at La Trinidad Medical Institute in Caracas for providing the experimental facility.

References

[1] Liu J. C. *et al.* (1975) SLAC-PUB-7404 .
[2] NCRP. (1984). NCRP report No. 79. Bethesda, MD. 19-21.
[3] Kase K.R *et al., Medical Accelerator. Health Phys*. **74**(1) (1998) 38-47.
[4] Vega-Carrillo H.R. *et al.* (2015). http://dx.doi.org/10.1016/j.apradiso.2015.05.004
[5] NCRP No. 116, (1993) Accessed June 2014, www.ncrponline.org/Publications.
[6] Yeh, J. J., and I. Lindau. "Atomic data and nuclear data tables." *Academic Press* 32 (1985) 1-155.
[7] Harvey R. R *et al.*, *Phys. Rev.* **136**, (1964) B126.

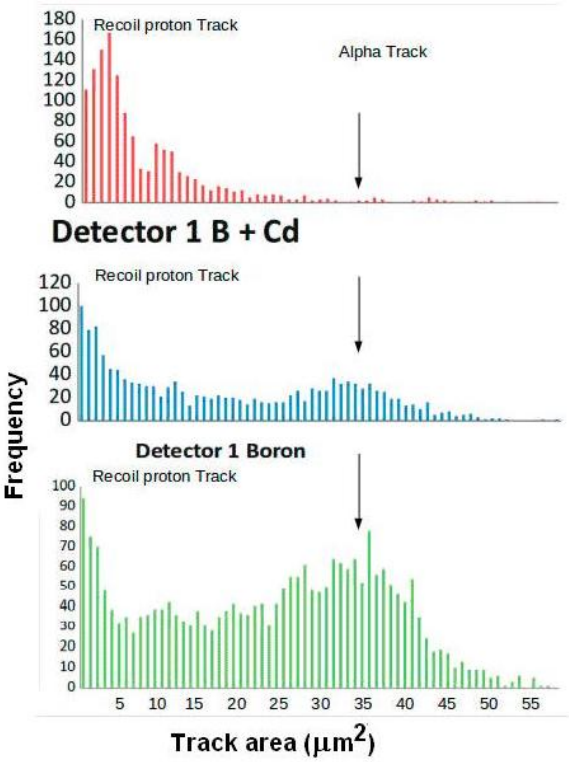

Fig.6. Track distributions. Frequency as function of the channel (track area in μm^2) is shown to illustrate how the thermal and epithermal components for photo-neutron field spectra can be discriminated.

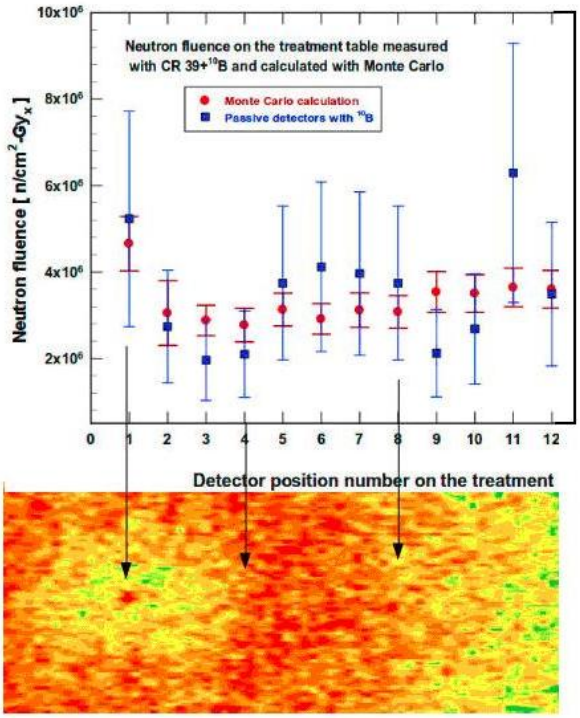

Fig.7. Comparison of results given by simulations and measurements. Areas delimited by arrows are related to photo-neutron fluence; It is highest at the isocenter (red spot at No. 1) then decreases (yellow area between the first two arrows) and then increases again with distance. After the third arrow it diminishes slowly.

[8] Fujibuchi T. *et al., Nucl. Instrum. Meth. Phys. Res. B* **349** (2015) 239-235.
[9] Vega-Carrillo H.R *et al., J. Radioanal. Nucl. Chem*., **283** 261-265.
[10] Esposito A., Bedogni R., Lembo L., Morelli M., *Radiat. Meas.* **43** (2008) 1038-1043.
[11] Kralik M., Turek K., Vondracek V. *Radiat. Prot. Dosim.* **132** (2008) 13-17.
[12] X-5 Monte Carlo Team. Los Alamos, NM. LANL report CP-03-0245
[13] F5 tally, Accessed June 2015, http://www.nucleonica.com/wiki/index.php?title=F5_tally
[14] Tossi G. *et al., Med. Phys*. **18** (1991) 54-60.
[15] Patil et al. Nucl. Instr. Meth. Phys. Res. B 269(2011)3261-3265.
[16] ICRP 60, Pergamon Press, Oxford, England, 1991.
[17] BEIR V, Health effects of exposure to low levels of ionizing radiation, National Academy Press,Washington, DC, 1990.
[18] Mameli A. *et al., Nucl. Instr. Meth. Phys. Res. B* **266** (2008) 3656–3660
[19] Castillo, R., J. Dávila, and L. Sajo Bohus. X Latin American Symp. on Nucl. Physics and Applications (2013)